

# GALACTICNUCLEUS: A high angular resolution $JHK_s$ imaging survey of the Galactic Centre

## II. First data release of the catalogue and the most detailed CMDs of the GC

F. Nogueras-Lara<sup>1</sup>, R. Schödel<sup>1</sup>, A. T. Gallego-Calvente<sup>1</sup>, H. Dong<sup>1</sup>, E. Gallego-Cano<sup>1,2</sup>, B. Shahzamanian<sup>1</sup>, J. H. V. Girard<sup>3</sup>, S. Nishiyama<sup>4</sup>, F. Najarro<sup>5</sup>, and N. Neumayer<sup>6</sup>

<sup>1</sup> Instituto de Astrofísica de Andalucía (CSIC), Glorieta de la Astronomía s/n, 18008 Granada, Spain e-mail: fnoguer@iaa.es

<sup>2</sup> Centro Astronómico Hispano-Alemán (CSIC-MPG), Observatorio Astronómico de Calar Alto, Sierra de los Filabres, 04550, Górgal, Almería, Spain

<sup>3</sup> Space Telescope Science Institute, Baltimore, MD 21218, USA

<sup>4</sup> Miyagi University of Education, Aoba-ku, 980-0845 Sendai, Japan

<sup>5</sup> Departamento de Astrofísica, Centro de Astrobiología (CSIC-INTA), Ctra. Torrejón a Ajalvir km 4, E-28850 Torrejón de Ardoz, Spain

<sup>6</sup> Max-Planck Institute for Astronomy, Königstuhl 17, 69117 Heidelberg, Germany

### ABSTRACT

**Context.** The high extinction and extreme source crowding of the central regions of the Milky Way are serious obstacles to the study of the structure and stellar population of the Galactic centre (GC). Surveys that cover the GC region (2MASS, UKIDSS, VVV, SIRIUS) do not have the necessary high angular resolution. Therefore, a high angular resolution survey in the near infrared is crucial to improve the state of the art.

**Aims.** Here, we present the GALACTICNUCLEUS catalogue, a near infrared  $JHK_s$  high angular resolution ( $0.2''$ ) survey of the nuclear bulge of the Milky Way.

**Methods.** We explain in detail the data reduction, data analysis, calibration, and uncertainty estimation of the GALACTICNUCLEUS survey. We assess the data quality comparing our results with previous surveys.

**Results.** We obtained accurate  $JHK_s$  photometry  $\sim 3.3 \times 10^6$  stars in the GC detecting around 20 % in  $J$ , 65 % in  $H$  and 90 % in  $K_s$ . The survey covers a total area of  $\sim 0.3$  square degrees, which corresponds to  $\sim 6000$  pc<sup>2</sup>. The GALACTICNUCLEUS survey reaches  $5\sigma$  detections for  $J \sim 22$  mag,  $H \sim 21$  mag and  $K_s \sim 21$  mag. The uncertainties are below 0.05 mag at  $J \sim 21$  mag,  $H \sim 19$  mag and  $K_s \sim 18$  mag. The zero point systematic uncertainty is  $\lesssim 0.04$  mag in all three bands. We present colour-magnitude diagrams for the different regions covered by the survey.

**Conclusions.**

**Key words.** Galaxy: centre – Galaxy: bulge – Galaxy: structure – stars: horizontal-branch – dust, extinction

## 1. Introduction

The Galactic centre (GC) is a main astrophysical target since it is the closest galactic nucleus located at only 8 kpc from Earth, about a hundred times closer than the Andromeda galaxy, and a thousand times closer than the next active galactic nucleus. The GC hosts a supermassive black hole (Sgr A\*) located at the dynamical centre of the Galaxy and surrounded by the nuclear star cluster, almost 10 times more massive than Sgr A\* (Launhardt et al. 2002; Schödel et al. 2014) and composed of a complex stellar population with the majority of the stars older than 5 Gyr (Pfuhl et al. 2011). On a larger scale, the NSC and Sgr A\* are embedded in, and form part of, the nuclear bulge (NB). The NB is a distinct stellar structure that stands clearly out from the kiloparsec-scale Galactic Bulge/Bar and constitutes a flattened, possibly disk-like structure -nuclear stellar disk (NSD)- with a radius of  $\sim 230$  pc and a scale height of  $\sim 45$  pc (Launhardt et al. 2002).

The GC is characterised by the most extreme conditions in the Galaxy: extreme stellar densities ( $\sim 10^{3-7}$  pc<sup>-3</sup>, Launhardt et al. 2002; Schödel et al. 2007, 2018), a tidal field so intense

that even massive, young clusters dissolve into the background in less than 10 Myr (Portegies Zwart et al. 2002), high turbulence and temperature of the interstellar medium (Morris & Serabyn 1996), a strong magnetic field (Crocker 2012), and intense UV radiation (Launhardt et al. 2002). Despite, or possibly because of these extreme properties, the GC is the Galaxy's most prolific massive star forming environment (Schödel et al. 2007; Yusef-Zadeh et al. 2009; Mauerhan et al. 2010).

The point cannot be overstressed that the centre of the Milky Way is the only galaxy nucleus in which we can actually resolve the NSC and the NB observationally and examine its properties and dynamics. Nevertheless, only small regions like the central parsec and the Arches and Quintuplet clusters, which supposes around 1% of the projected area, have been explored in detail.

To characterise the GC stellar population it is necessary to overcome the high stellar crowding and the extreme interstellar extinction ( $A_V \gtrsim 30$ ,  $A_{K_s} \gtrsim 2.5$ , e.g. Scoville et al. 2003; Nishiyama et al. 2008; Fritz et al. 2011; Schödel et al. 2010; Nogueras-Lara et al. 2018a). This requires an angular resolution of  $\sim 0.2''$  and multi-band observations. Several large imaging surveys include the GC region (e.g., 2MASS, UKIDSS, VVV,

SIRIUS/IRSF), but they are limited in angular resolution to  $> 0.6''$  by atmospheric seeing. Hence, their photometry is inaccurate and their completeness limit is as shallow as  $K \sim 14$  mag. Additionally, stars brighter than  $K \approx 9 - 10$  mag are usually heavily saturated in these surveys.

In this paper we present the first data release of the GALACTICNUCLEUS survey, a high angular resolution  $\sim 0.2''$ , multi-wavelength ( $J$ ,  $H$  and  $K_s$ ) imaging survey especially designed to observe the GC. It constitutes the first survey of the central regions of our Galaxy with  $\sim 10$  mag dynamic range in three bands in the near infrared (NIR). Several papers that use the GALACTICNUCLEUS survey and show its potential have already been published (Nogueras-Lara et al. 2018a,b) or submitted (Gallego-Cano et al., submitted; Nogueras-Lara et al., submitted).

This paper constitutes the second paper of a series initiated with Nogueras-Lara et al. (2018a).

## 2. Observations

The GALACTICNUCLEUS survey consists of 49 pointings toward the Galactic Centre and the inner Bulge (Fig 1). The observations were carried out with HAWK-I (High Wide field K-band Imager, Kissler-Patig et al. 2008) located at the ESO VLT unit telescope 4<sup>1</sup>. We used the broadband filters  $J$ ,  $H$  and  $K_s$  to cover the NIR regime. HAWK-I has four HAWAII 2RG 2048  $\times$  2048 detectors (four chips) with a cross-shaped gap of  $15''$  between them. The on-sky field of view of HAWK-I is  $7.5' \times 7.5'$  and its pixel scale is  $0.106''/\text{pixel}$ . We used the fast photometry mode to obtain series of short exposure frames with an exposure time of  $DIT = 1.26$  s (detector integration time) that allowed us to improve the angular resolution of the final images to  $\sim 0.2''$  through applying the speckle holography algorithm (Schödel et al. 2013). Due to the short readout time, we had to window the detector, which resulted in a field of view (FoV) of  $2048 \times 768$  pixels for each of the four chips. Tables A.1, A.2, and A.3 summarise the observing conditions for each pointing.

### 2.1. Observing strategy

We treated each of the four HAWK-I detectors in a completely independent way. To cover the gap between the detectors and to achieve some overlap between the pointings, we applied random jittering with a jitter box varying from  $30''$  (2015 data) to  $1'$  (2016-2018 data) width. The jitter box was increased after the first epoch to optimise the data coverage in the cross-shaped gap.

The 49 pointings cover the Galactic Centre in four distinct groups: (1) A continuous, rectangular area of about  $36' \times 16'$  centred on Sgr A\* (30 pointings, labelled as 1-30), (2) eleven pointings (D9-D15, D17-D19 and D21) toward the east and west of the central field to cover low-extinction areas in the central part of the nuclear stellar disk, (3) four pointings (T3, T4, T7 and T8) in the transition zone between the NB and the inner bulge, and (4) four pointings (B1, B2, B5 and B6) toward comparison fields in the inner bulge just north of the nuclear disc. The entire survey area is outlined in Fig. 1, while Fig. 2 allows an identification of each pointing. All pointings overlap with at least one adjacent pointing. In this way, we were able to compare the common stars to assess the data quality.

We rotated HAWK-I  $31.40^\circ$  east of north to align the observed fields with the Galactic Plane (Reid & Brunthaler 2004). Due to the extreme source density toward the GC simple jittering

<sup>1</sup> Based on observations made with ESO Telescopes at the La Silla Paranal Observatory under programme ID 195.B-0283

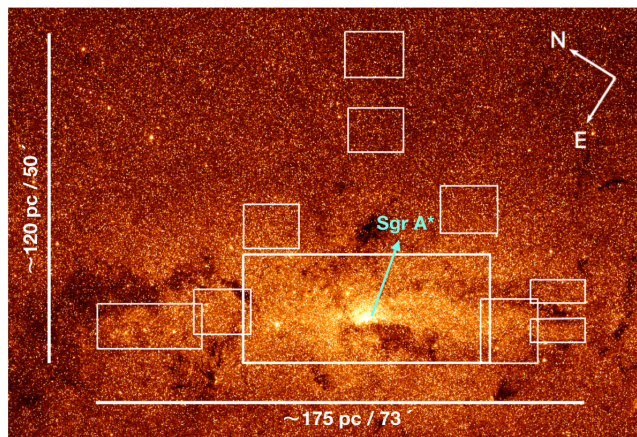


**Fig. 1.** Scheme of the target fields for the GALACTICNUCLEUS survey over-plotted on a Spitzer/IRAC image at  $3.6 \mu\text{m}$ . The position of Sagittarius A\* is highlighted in cyan.

on target will not work to obtain accurate measurements of the sky background. Instead, we chose the following strategy: Sky frames were taken just before or after each science observation on a dark cloud with very low stellar density located approximately at  $17^h 48^m 01.55^s$ ,  $-28^\circ 59' 20''$ . We rotated the camera  $70^\circ$  east of north to align the rectangular FoV with the extension of the dark cloud. From the sky observations we created a master sky frame. We then scaled the master sky to the instantaneous sky background of each exposure, which was estimated from the median value of the 10% of pixels with the lowest values. A detector dark image was subtracted from both the master sky and from each reduced science frame before determining this scaling factor (see also Nogueras-Lara et al. 2018a, for a detailed description of the methodology).

## 3. Data reduction and analysis

The reduction and treatment of the central pointing of the survey (F1) was described in detail in Nogueras-Lara et al. (2018a). The same procedure was used for the whole survey. Briefly summarised, it consists of the following steps:

1. Standard reduction: Dark subtraction, flat fielding, sky subtraction and bad pixel correction. We also aligned the frames correcting for the jittering.
2. Distortion correction: We used stellar positions from VVV  $J$ -band images to compute a geometric distortion solution for each of the bands and fields observed.
3. Speckle holography: We used the speckle holography method (see e.g. Primot et al. 1990; Petr et al. 1998) optimised for crowded fields (Schödel et al. 2013). This is an image reconstruction technique that combines a high number of short exposure frames ( $\sim 1000$  per pointing in our case) using an averaged division of quantities in Fourier space (eq. 1, Schödel et al. 2013). The final product is convolved with a Gaussian of FWHM (full width at half maximum) of  $0.2''$ . This determines the final angular resolution of the catalogue. Since this technique requires the knowledge of the instantaneous PSF of each exposure, which can vary spatially due to anisoplanatic effects, we divided each frame into small subregions and used the reference stars in each of them to extract local, instantaneous PSFs (see detailed description in Sec. 2.3 of Nogueras-Lara et al. 2018a).

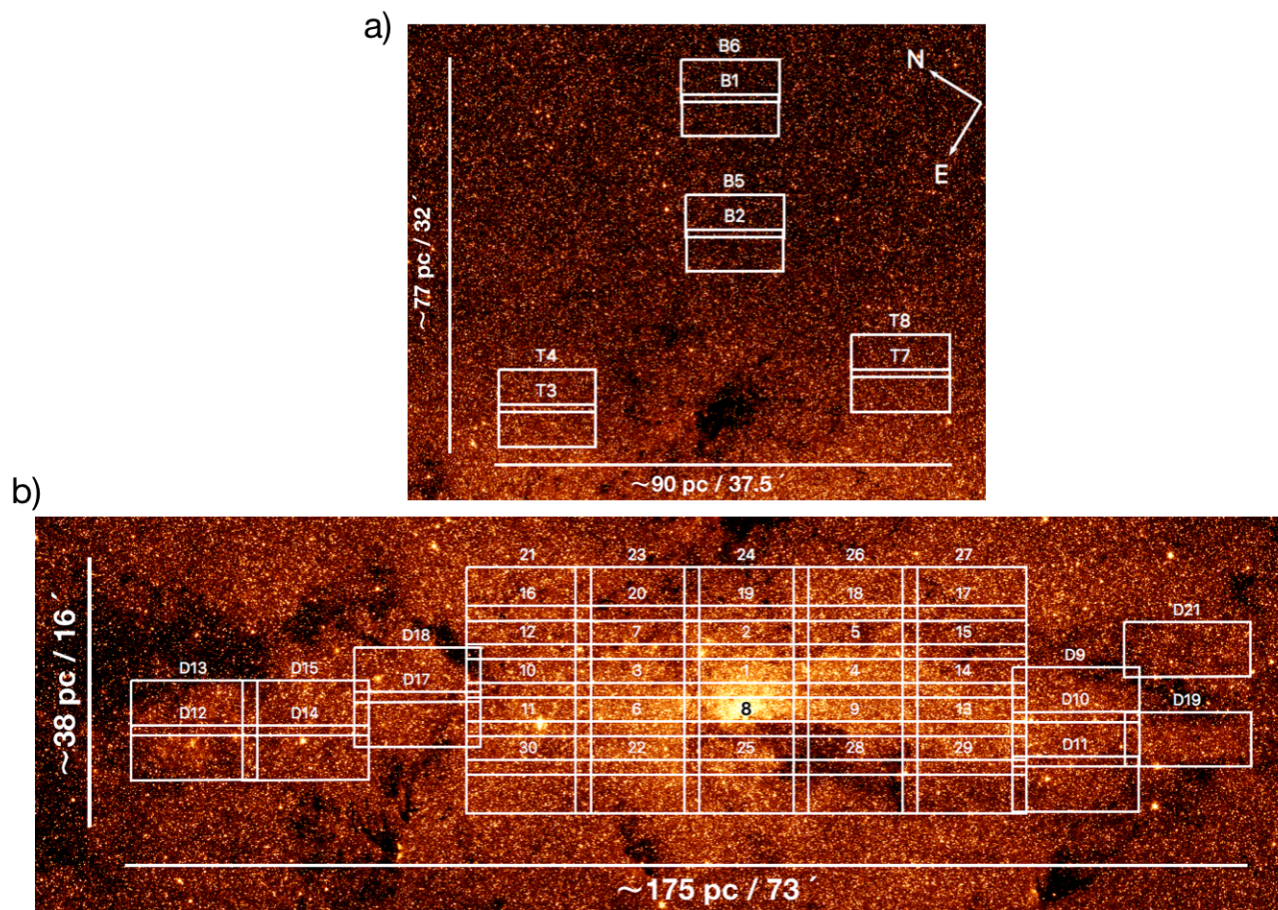


**Fig. 2.** Detailed scheme of all the fields observed in the GALACTICNUCLEUS survey. Each white square represent a field of the survey. Labels are included in white to identify the fields. Fields in the NSD, inner Galactic bulge, and transition zone between the bulge and the centre are identified by the letters 'D', 'B' and 'T'. Fields in the central region are identified by numbers from 1 to 30.

4. Photometry: we used the *StarFinder* software package (Diolaiti et al. 2000) to perform PSF photometry and astrometry for each chip independently using the final holographic product. Since *StarFinder* underestimates the uncertainties computed for individual stars (Emiliano Diolaiti, private communication), we used an alternative approach. We generated three independent holographic images for each chip (sub-images) using 1/3 of the data for each of them. We also created a deep final image using all the data available. We extracted PSF photometry from each sub-image and from the deep one. We accepted a star only if it was detected in all three sub-images. We calculated the final flux of each star using the deep image and the uncertainty by means of the equation (Nogueras-Lara et al. 2018a):

$$\Delta f = \frac{f_{max} - f_{min}}{2\sqrt{N}}, \quad (1)$$

where  $f_{max}$  and  $f_{min}$  are the maximum and minimum fluxes obtained for each star in the sub-images and  $N = 3$  is the number of sub-images.

This strategy is quite conservative, but it allows us to keep only real detections and to estimate the uncertainties based on three independent data sets. We also considered the possible variation of the PSF across the detector. We divided each

chip into three equal regions from which we extracted three independent PSFs. We estimated the uncertainty associated to its variation by comparing the PSFs computed for each region (for details, see Sec. 3.1.2 of Nogueras-Lara et al. 2018a). For all the 49 pointings and each individual chip, this PSF uncertainty is  $\lesssim 0.025$  mag in all three bands. We added this uncertainty quadratically to the statistical uncertainty that was determined from the three sub-images.

5. Calibration: We computed the astrometric solution by using common stars between each chip and the VVV catalogue. We estimated the uncertainty of this procedure to  $\lesssim 0.05$  arcseconds. The photometric calibration was carried out with stars common with the SIRIUS/IRSF GC survey (e.g. Nagayama et al. 2003; Nishiyama et al. 2006a), designed specially for the study of the GC. We used bright stars (non-saturated) with low uncertainties  $< 0.05$  mag in all three bands in our catalogue.
6. Field combination: We obtained the final list of stars for each filter and pointing by combining the stars detected on each chip. We corrected the small shifts in magnitude that can appear between the chips by using stars in the overlap region of all four of them and finding the factor for each chip that minimised the overall  $\chi^2$  (for further details, see Dong et al. 2011; Nogueras-Lara et al. 2018a). We then combined the

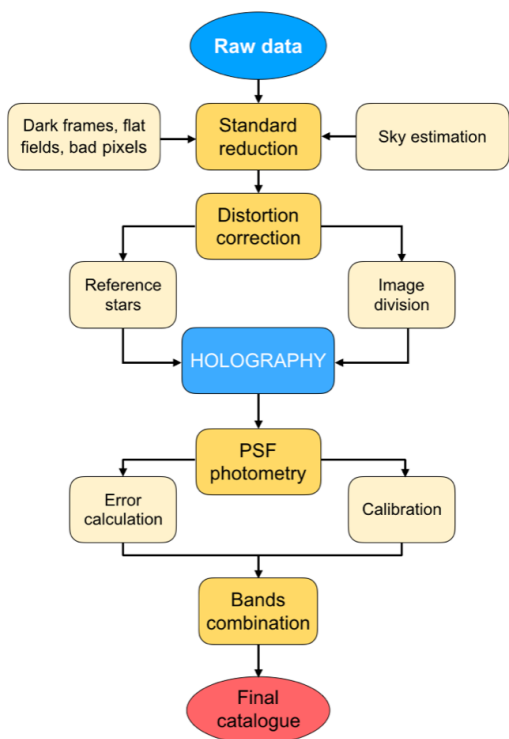


**Fig. 3.** Scheme of the obtention of the final catalogue for each chip.

star lists of the four chips. For stars detected in more than one chip we computed their photometry as the mean of the detections and their uncertainties as the quadratic combination of each uncertainty. After this procedure, we recalibrated the final star list of each pointing with SIRIUS/IRSF GC survey to take care of any photometric offsets that might have been introduced during the process. Finally, we combined all three bands and generated a catalogue for each field. Figure 3 shows a scheme of the whole process.

## 4. Preparation of the catalogues

We prepared several catalogues: 1) Four catalogues for the regions (consisting of two pointings each) shown in Fig. 2a). They correspond to the inner bulge and the transition region between the inner bulge and the NB. 2) Three catalogues for the central region shown in Fig. 2b): GC West (pointings D12 to D18), GC Central (pointings 1 to 30), and GC East (pointings D9 to D11, D19 and D21).

### 4.1. Astrometry

For each band, we identified common stars in the overlapping regions and computed their positions through averaging the multiple detections. The final catalogue was created by combining all three bands. The maximum allowed offset for a star present in different bands was set to  $\sim 0.1''$ , half the angular resolution of the images. The final positions of the stars detected in more than one band were computed as the mean positions of the individual detections. The absolute astrometric uncertainty derives from the alignment with the VVV stars that were used to compute the astrometric solution. We estimated an upper limit of the

**Table 1.** Fields included in each catalogue.

Catalogue	Fields included
Central	1-30
NSD East	D12-D18
NSD West	D9-D11, D19, D21
Transition East	T3-T4
Transition West	T7-T8
Inner Bulge North	B1,B6
Inner Bulge South	B2,B5

**Notes.** The name of each field stars by a capital letter that indicates its position in the survey: 'D' -> Nuclear stellar disk, 'B' -> Inner bulge, 'T'-> transition zone inner bulge-nuclear stellar disk and ' ' for the fields in the central part of the survey.

absolute astrometric uncertainty of  $0.05''$  with respect to VVV. As concerns the relative astrometric uncertainty of the stars, we examined the following sources of uncertainty: 1) Uncertainties derived from the measurements in the three independent sub-images for each band and pointing (see Sec. 3). 2) Uncertainties measured from the common stars in the overlapping area between the four chips for each pointing. 3) Uncertainties estimated from common stars when combining the different pointings to produce the final list for each band. 4) Uncertainties estimated from the combination of the positions of the stars from the three different bands. Figure 4 shows the corresponding uncertainties for chips, pointings, and the central catalogue for the case of the *J*-band. We concluded that the relative astrometric uncertainty is dominated by the combination of the different pointings and bands (points 3 and 4 above).

The final catalogues include the uncertainty due to 3) and 4) for the case of stars detected in more than one field and/or detected in more than one band. For the remaining stars we estimated an upper limit of  $\sim 45$  mili-arcsec that is the maximum value obtained in the analysis presented in Fig. 4.

### 4.2. Photometry

For stars detected in more than one pointing we computed the mean flux as the average value of the individual detections and estimated the photometric uncertainty by means of the quadratic propagation of the individual uncertainties of each detection. We compared the uncertainties derived from multiple detections with the one determined from the measurements in the three sub-images (Eq. 1). We used a two sigma clipping algorithm to calculate the mean of the uncertainties obtained with both methods and concluded that both values are similar for all three bands ( $\sim 0.03$  mag). Figure 5 shows the uncertainties obtained using both methods.

For the combination of the pointings, we recomputed the zero point (ZP) using the Sirius catalogue when adding new pointings to the final catalogue. In this way, we avoided small photometric shifts that can appear when computing the average values for common stars.

We ended up with an uncertainty  $\leq 0.05$  mag for all three bands at  $J \lesssim 21$  mag,  $H \lesssim 19$  mag and  $K_s \lesssim 18$  mag, which is slightly better than for the case of the F1 alone (the central

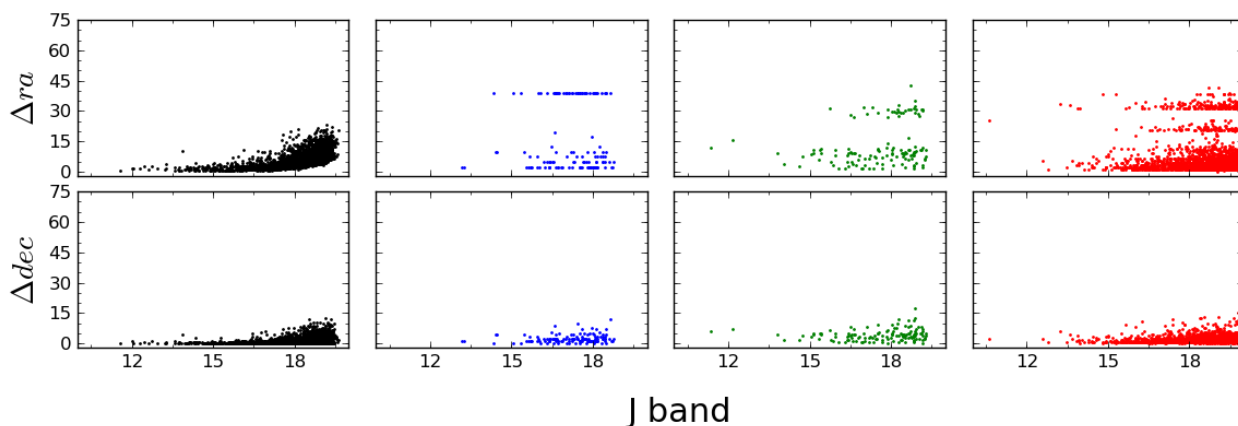


**Fig. 4.** Analysis of the astrometric uncertainties for the  $J$ -band. The y-axes have units of milli-arcseconds. Each column depicts the uncertainties associated to: 1) Relative astrometry measured on a single chip and pointing (F6, chip1 is shown as an example). 2) Combination of chips for a given pointing (F6 shown as an example). 3) Combination of all fields for the central region. 4) Combination of the three different bands for the central region. The plots in columns 2, 3 and 4 show steps in the distributions which are caused by systematic offsets between different chips, pointings, and filters.

most field that suffers the worst crowding) that was analysed in Nogueras-Lara et al. (2018a).

#### 4.2.1. Calibration

To calibrate GALACTICNUCLEUS, we used the near infrared  $JHK_s$  SIRIUS IRSF survey (e.g. Nagayama et al. 2003; Nishiyama et al. 2006a). This catalogue was specially designed to study the GC and it uses PSF photometry, which allows to improve the photometry in crowded fields. Thus, its characteristics make this survey a very appropriate reference. Moreover, we have compared both photometric systems to check whether there is any significant difference between the filters:

- We computed the effective wavelength obtained for a RC (red clump) star located at the GC distance with an extinction of  $A_{K_s} \sim 1.9$  mag, corresponding to the extinction expected at the GC (Nogueras-Lara et al. 2018a). We obtained that the effective wavelength for the equivalent filters differs by  $\lesssim 0.5\%$ .
- We also calculated the photometry in both photometric systems for a RC star and an early type star ( $T = 45\,000$  K) located at the GC distance and assuming an extinction of  $A_{K_s} \sim 1.9$  mag. We obtained that the difference is  $\lesssim 0.8\%$  in all three bands.

Therefore, we concluded that the differences between both photometric systems are negligible.

#### 4.2.2. Zero point

Once produced the final lists for each band, we recomputed the ZP using again the SIRIUS/IRSF GC survey. This calibration was done in the same way as explained in Nogueras-Lara et al. (2018a). We identified non-saturated common stars (coincident in position within a radius of  $\sim 0.1''$ ). Moreover, in order to use only isolated stars, we excluded all sources with a secondary star within  $\sim 0.5''$  in the GALACTICNUCLEUS catalogue (SIRIUS is a seeing-limited survey with an angular resolution  $\sim 1''$ ). We

excluded all stars with an uncertainty  $> 0.05$  mag in the GALACTICNUCLEUS catalogue or  $> 0.1$  mag in the SIRIUS catalogue. The calculation of the ZP was done using a 2-sigma clipping algorithm to remove outliers. Figure 6 shows all the common stars and those selected for calibration.

#### 4.2.3. Zero point uncertainties

To estimate the uncertainties of the ZPs, we took several effects into account: 1) The ZP uncertainty associated to the SIRIUS catalogue, 0.03 mag in all three bands (Nishiyama et al. 2006b, 2008). 2) The process to combine the chips and pointings until obtaining the final catalogue is complex and may lead to additional systematic uncertainties of the ZP. Figure 7 shows the comparison between the common stars in all three bands between the central and the NSD East and West catalogues. The uncertainties were computed using eq. 1. From this comparison we estimated an upper limit for the differential ZP uncertainty of  $\sim 0.03$  mag in all three bands using a two sigma clipping algorithm. This is consistent with the uncertainty estimated in Nogueras-Lara et al. (2018a) for the central field obtained comparing the observations taken for the central field of the survey (F1) and observations of the same region from a pilot study using also the speckle holography technique. 3) Statistical uncertainty of the ZPs: The high number of stars used for the ZP calibration at each band results in a negligible statistical uncertainty.

Combining quadratically the uncertainties due to 1) and 2) we ended up with an uncertainty of the ZP of 0.04 mag in all three bands, which is in agreement with the value of 0.036 mag that was obtained for the central field in Nogueras-Lara et al. (2018a).

#### 4.3. Completeness

Given the high number of sources detected, using the standard approach of inserting artificial stars would increase enormously the computational time needed to analyse the regions covered. Instead of this, we have used an alternative approach based on the determination of the critical distance from a bright star at which we are able to detect a star of any given magnitude (Eisenhauer et al. 1998; Harayama et al. 2008). This information is

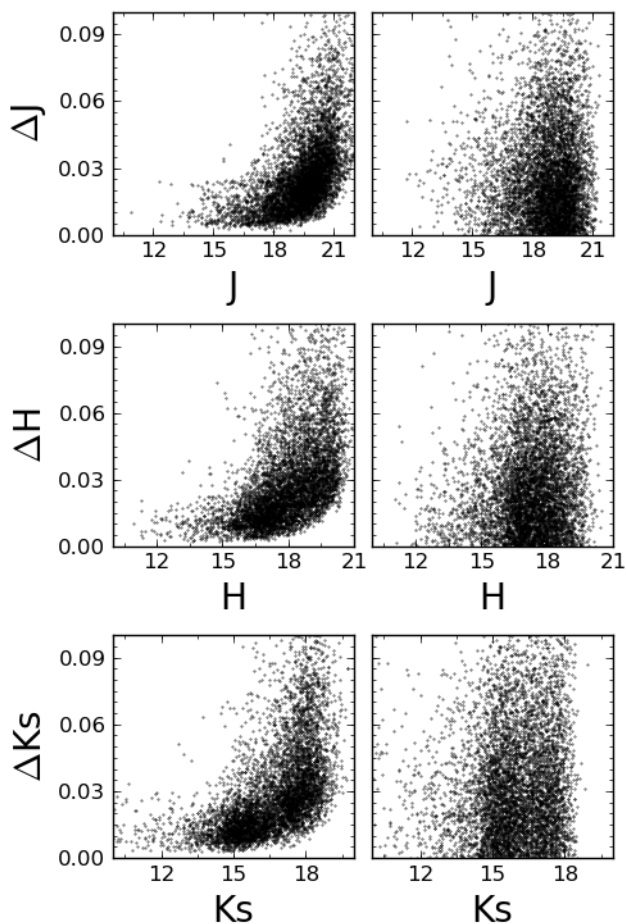


**Fig. 5.** Left panels: photometric uncertainties due to the quadratic propagation of the errors for each star. Right panels: uncertainties computed for stars detected in the overlapping regions between fields using eq. 1. The uncertainties shown in the right panels reach less deep magnitudes since those stars need to be detected in more than one field, and the slightly different atmospheric conditions between pointings complicate the detection of the faintest stars. Only a random fraction of the stars has been plotted for clarity.

later translated to completeness maps for each magnitude bin considered. This technique assumes that the detection probability of a single star is constant across the analysed field. Since our final catalogues are produced combining independent pointings that were obtained under non-uniform observing conditions and since the stellar density varies as a function of position in the GC, we analysed the completeness due to crowding on smaller subregions of  $2' \times 1.4'$ . For a rough assessment of overall completeness, we subsequently averaged over all the subregions. We applied this technique only to the central pointings (1-15) as they are the most challenging ones in terms of crowding. Crowding is the factor that dominates completeness in the sensitive  $K_s$ - and  $H$ -band images. We estimated a completeness of  $\sim 80\%$  at  $K_s \sim 16$  mag and  $H \sim 18$  mag. Crowding is hardly an issue in the  $J$ -band images because the much higher interstellar extinction (note that the reddening induced colours  $J - K_s \approx 5$  at the GC) at short NIR wavelengths reduces the number of de-

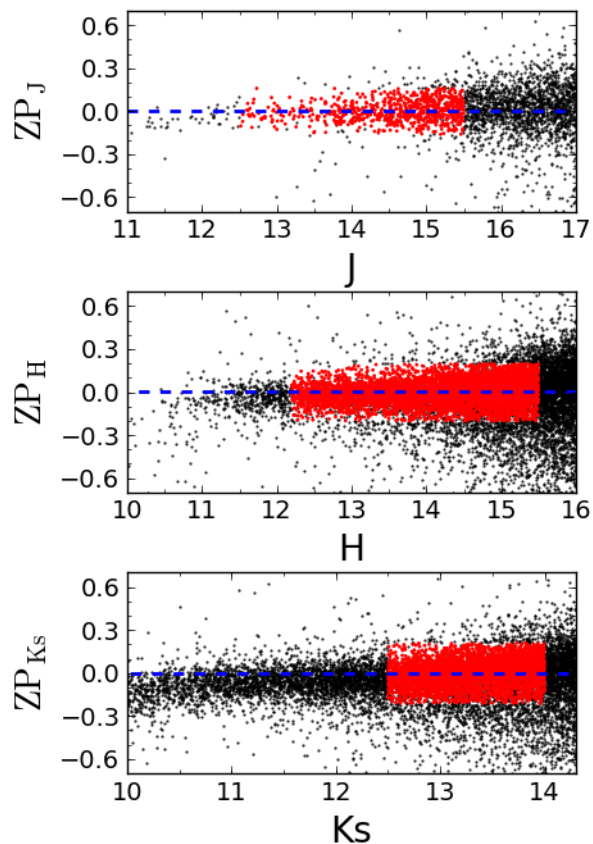


**Fig. 6.** Comparison of the photometry of GALACTICNUCLEUS and SIRIUS stars after obtaining the final lists for each band in the central catalogue. All common stars between SIRIUS and GALACTICNUCLEUS are plotted in black. Red points indicate those used for calibration. The deviation for bright stars is caused by saturation.

tected stars considerably. We run artificial stars tests in the central pointing of the central catalogue (F1), the most crowded one, and obtained a completeness of  $\sim 80\%$  at  $J \sim 20$  mag. This is a conservative limit for completeness due to crowding because most other fields will be less crowded.

We also run the same simulations for  $H$  and  $K_s$  bands and confirmed the limits previously obtained. Moreover, a comparison with the deeper photometry obtained for the nuclear star cluster in  $H$  and  $K_s$  ( $\sim 0.06''$  angular resolution) with NACO/VLT (Gallego-Cano et al. 2018), agrees with the completeness limits that we estimated here.

#### 4.4. Final catalogues

We obtained accurate photometry in the NIR  $J$ ,  $H$  and  $K_s$  bands for  $\sim 3.3 \times 10^6$  stars. Approximately 20% of them were detected in  $J$ , 65% in  $H$  and 90% in  $K_s$ . The catalogue covers a total area of  $\sim 0.3$  square degrees, which corresponds to  $\sim 6000$  pc<sup>2</sup>. This supposes an average stellar density of  $\sim 600$  stars/pc<sup>2</sup>.

The final catalogues published in this paper include 25 columns that contain information about:

- **Position and uncertainties between bands:** right ascension and declination expressed in degrees (columns 1 and

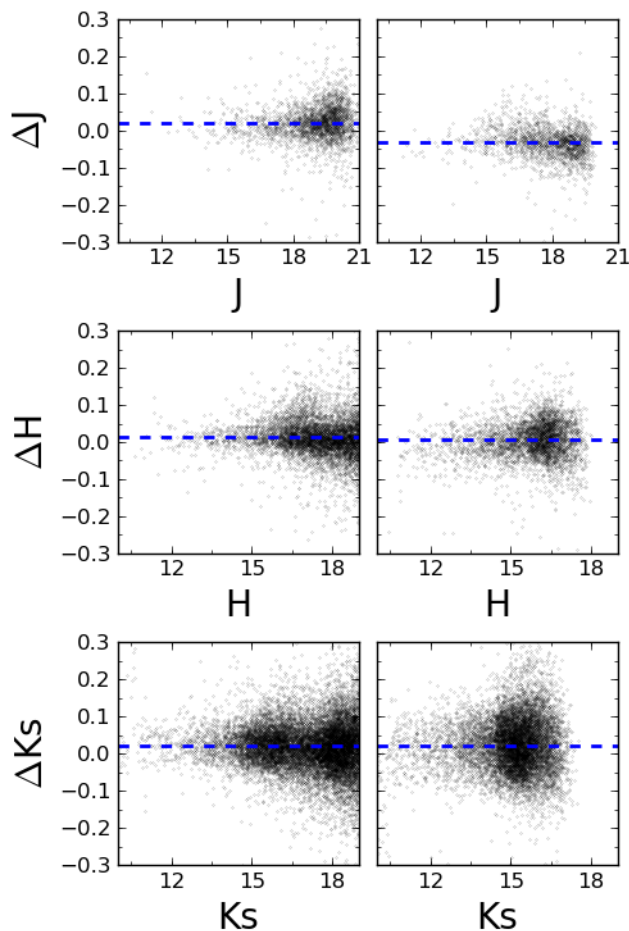


**Fig. 7.** Left panels: photometric comparison of the common stars between the central and the NSD East catalogues. Right panels: photometric comparison Central-NSD West catalogues. The uncertainties have been calculated using eq. 1. The blue dashed line indicates the mean offset existing between the considered regions.

3) and their corresponding uncertainties expressed in arcseconds (columns 2 and 4). For stars detected in more than one band these coordinates have been calculated averaging the positions of the detections. The uncertainties refer to the deviation of the measurements (see column 4 in Fig. 4). For stars detected in a single band, we indicated the corresponding coordinates and the uncertainty associated to the detection (see column 3 in Fig. 4).

- **Relative position and uncertainties for each band:** We included the positions and the associated uncertainties estimated from multiple detections of the same star in different pointings within the same band (column 3 in Fig. 4). The positions are expressed in degrees and the uncertainties in units of arcseconds (columns 5-8 for  $J$ , 9-12 for  $H$ , 13-16 for  $K_s$ ). A value of zero means that a star was not detected in a given band or that it was not detected multiple times in overlapping pointings. In those cases we refer to the upper limit of 45 milli-arcsec derived previously (Sec. 4.1).

- **Photometry and uncertainty for each band:** For each star we included the photometry in  $J$ ,  $H$ , and  $K_s$  and the associated uncertainties expressed in mag (columns 17-22). A value of 99 indicates a non-detection.

- **Number of multiple detections:** This value indicates the number of multiple detections in overlapping pointings for each band (columns 23, 24, 25).

Table 2 outlines the first rows of the central catalogue specifying the columns described previously.

Figure 8 shows an RGB image corresponding to the GC Central catalogue produced from a mosaic of pointings 1 to 30.

The catalogues described in this paper are made publicly available at the CDS via anonymous ftp to cdsarc.u-strasbg.fr or via <http://cdsarc.u-strasbg.fr/>. Moreover, we are now preparing the individual catalogues for each chip and band for the ESO phase three data release of our ESO Large Programme that underlies this catalogue. The data will be available from the ESO Science Archive.

## 5. Quality assessment

We carried out several tests to check the photometric quality of our catalogues:

### 5.1. Comparison with SIRIUS catalogue

We compared the photometry obtained for all three bands with the SIRIUS IRSF survey catalogue. To check that the ZP does not change significantly across the final region covered by the catalogues when combining the different fields. For this purpose we used the GC Central catalogue, which we expect to make a good test case because it contains the most complex region and combines 30 different pointings observed under different seeing conditions at different epochs (see table A.1). We cross-matched both catalogues and identified common stars in all three bands. We divided the GC central region into four independent vertical columns, from east to west along the Galactic Plane, and analysed them independently. We used eq. 1 for comparing the photometry. Figure 9 shows the results. We calculated the offset using a two sigma clipping algorithm to remove outliers and avoiding saturated and too faint stars. We considered stars of  $J = 12.5 - 15.5$  mag,  $H = 12.3 - 15.5$  mag, and  $K_s = 12.5 - 14$  mag (see also Fig. 6). We then computed the difference between the maximum and minimum offsets for each band between the 4 different columns. This difference is  $< 0.01$  mag in all three bands. We conclude that there is no significant variability of the ZP across the GC Central field.

### 5.2. Comparison with a previously used sub-catalogue

We compared the final GC Central catalogue with a previous version that included only 14 of 30 fields and that was used in previous work (Nogueras-Lara et al., submitted; Gallego-Cano et al., submitted). The main difference introduced by the final version is the photometry of the common stars detected in pointings that were not included in the former version. Also, the ZPs computed at intermediate steps could have varied (see Sec 4.2) because less fields were present in the previous version of the GC Central catalogue. Figure 10 shows the comparison between the preliminary and the final catalogues following eq. 1.

**Table 2.** Fields included in each catalogue.

ra	Δra	dec	Δdec	ra <sub>J</sub>	Δra <sub>J</sub>	dec <sub>J</sub>	Δdec <sub>J</sub>	ra <sub>H</sub>	Δra <sub>H</sub>	dec <sub>H</sub>	Δdec <sub>H</sub>	ra <sub>K<sub>s</sub></sub>	Δra <sub>K<sub>s</sub></sub>	dec <sub>K<sub>s</sub></sub>	Δdec <sub>K<sub>s</sub></sub>	J	dJ	H	dH	K <sub>s</sub>	dK <sub>s</sub>	i <sub>J</sub>	i <sub>H</sub>	i <sub>K<sub>s</sub></sub>	
°	"	°	"	°	"	°	"	°	"	°	"	°	"	°	"	mag	mag	mag	mag	mag	mag				
266.47	0.004	-28.97	0.002	266.47	0.012	-28.97	0.006	266.47	0.005	-28.97	0.003	266.48	0.007	-28.97	0.003	11.355	0.008	10.666	0.008	10.409	0.006	4	3	3	
266.47	0.003	-28.97	0.001	266.47	0.016	-28.97	0.007	266.47	0.012	-28.97	0.006	266.48	0.008	-28.97	0.004	12.148	0.009	11.721	0.007	11.556	0.007	4	4	4	
266.47	0.001	-28.98	0.000	266.47	0.009	-28.98	0.004	266.47	0.008	-28.98	0.004	266.47	0.011	-28.98	0.005	13.813	0.008	12.697	0.007	12.340	0.011	4	4	4	
266.48	0.009	-28.96	0.004	266.48	0.004	-28.96	0.002	266.48	0.009	-28.96	0.004	266.48	0.005	-28.96	0.003	14.063	0.006	13.524	0.015	13.411	0.008	3	4	3	
266.47	0.005	-28.97	0.002	266.47	0.003	-28.97	0.002	266.47	0.013	-28.97	0.006	266.47	0.011	-28.97	0.005	14.612	0.011	13.848	0.014	13.621	0.006	4	4	4	
266.48	0.002	-28.97	0.001	266.48	0.008	-28.97	0.004	266.48	0.000	-28.97	0.000	266.48	0.011	-28.97	0.005	14.753	0.009	12.861	0.006	12.051	0.008	4	4	4	
266.48	0.001	-28.97	0.000	266.48	0.008	-28.97	0.003	266.48	0.011	-28.97	0.005	266.48	0.005	-28.97	0.002	15.037	0.008	12.949	0.007	11.968	0.005	4	4	4	
266.48	0.011	-28.97	0.006	266.48	0.009	-28.97	0.004	266.48	0.013	-28.97	0.005	266.48	0.043	-28.97	0.012	15.146	0.009	14.287	0.011	13.961	0.032	4	4	4	
266.47	0.012	-28.97	0.002	266.47	0.011	-28.97	0.005	266.47	0.002	-28.98	0.001	266.47	0.037	-28.97	0.006	15.139	0.024	11.580	0.010	10.167	0.015	3	2	2	
266.47	0.011	-28.96	0.005	266.47	0.006	-28.96	0.002	266.47	0.004	-28.96	0.001	266.47	0.038	-28.96	0.010	15.328	0.012	11.605	0.010	10.029	0.021	3	3	2	
266.48	0.004	-28.97	0.002	266.48	0.011	-28.97	0.005	266.48	0.005	-28.97	0.002	266.48	0.009	-28.97	0.004	15.389	0.008	14.787	0.008	14.575	0.011	4	4	4	
266.48	0.003	-28.97	0.001	266.48	0.009	-28.97	0.004	266.48	0.009	-28.97	0.004	266.48	0.003	-28.97	0.001	15.405	0.007	13.721	0.007	12.859	0.006	4	4	4	
266.47	0.001	-28.97	0.000	266.47	0.011	-28.97	0.005	266.47	0.010	-28.97	0.004	266.47	0.005	-28.97	0.002	15.424	0.008	14.649	0.007	14.400	0.005	4	4	4	
266.47	0.011	-28.96	0.002	266.47	0.032	-28.96	0.007	266.47	0.029	-28.96	0.001	266.47	0.008	-28.96	0.004	15.735	0.010	12.232	0.008	10.437	0.014	4	4	4	
266.48	0.002	-28.96	0.001	266.48	0.005	-28.96	0.002	266.48	0.009	-28.96	0.004	266.48	0.003	-28.96	0.001	15.762	0.011	14.748	0.007	14.362	0.024	4	4	4	
266.48	0.011	-28.97	0.002	266.48	0.003	-28.97	0.001	266.48	0.027	-28.98	0.009	266.48	0.027	-28.97	0.009	15.851	0.008	14.989	0.007	14.701	0.010	4	4	4	
266.48	0.002	-28.97	0.001	266.48	0.011	-28.97	0.005	266.48	0.014	-28.97	0.007	266.48	0.009	-28.97	0.004	15.946	0.008	15.030	0.007	14.695	0.005	4	4	4	
266.48	0.002	-28.97	0.001	266.48	0.008	-28.97	0.004	266.48	0.005	-28.97	0.002	266.48	0.006	-28.97	0.003	15.960	0.008	13.629	0.007	12.568	0.009	4	4	4	
266.48	0.004	-28.97	0.002	266.48	0.002	-28.97	0.001	266.48	0.011	-28.97	0.005	266.48	0.013	-28.97	0.006	16.069	0.009	15.204	0.011	14.895	0.009	4	3	3	
266.48	0.013	-28.97	0.007	266.48	0.005	-28.97	0.003	266.48	0.038	-28.97	0.013	266.48	0.035	-28.97	0.009	16.538	0.038	15.649	0.058	15.854	0.038	3	2	3	
266.47	0.001	-28.97	0.000	266.47	0.005	-28.98	0.002	266.47	0.004	-28.98	0.002	266.47	0.005	-28.98	0.002	16.371	0.008	15.469	0.007	15.267	0.030	4	3	4	
266.48	0.006	-28.97	0.003	266.48	0.002	-28.97	0.001	266.48	0.013	-28.97	0.006	266.48	0.008	-28.97	0.004	16.310	0.008	12.450	0.007	10.500	0.010	4	3	4	
266.47	0.008	-28.97	0.004	266.47	0.008	-28.97	0.003	266.47	0.011	-28.97	0.005	266.47	0.003	-28.97	0.002	16.395	0.017	15.688	0.022	15.505	0.010	4	4	3	
...	...	...	...	...	...	...	...	...	...	...	...	...	...	...	...	...	...	...	...	...	...	...	...	...	...

**Notes.** First rows of the central catalogue, ra, Δra and dec, Δdec are the right ascension and the declination of the sources (and their corresponding uncertainties) obtained combining the detections in several bands. ra<sub>J</sub>, Δra<sub>J</sub> and dec<sub>J</sub>, Δdec<sub>J</sub> correspond to the coordinates and uncertainties for any single band, *i*. The coordinates were rounded to two decimals in this table. *J*, *dJ*, *H*, *dH*, *K<sub>s</sub>* and *dK<sub>s</sub>* are the photometry and the associated uncertainties. A 99 indicates that there is no detection for a given source. *i<sub>J</sub>*, *i<sub>H</sub>* and *i<sub>K<sub>s</sub></sub>* indicate the number of fields where a star were detected to obtain its final photometry.

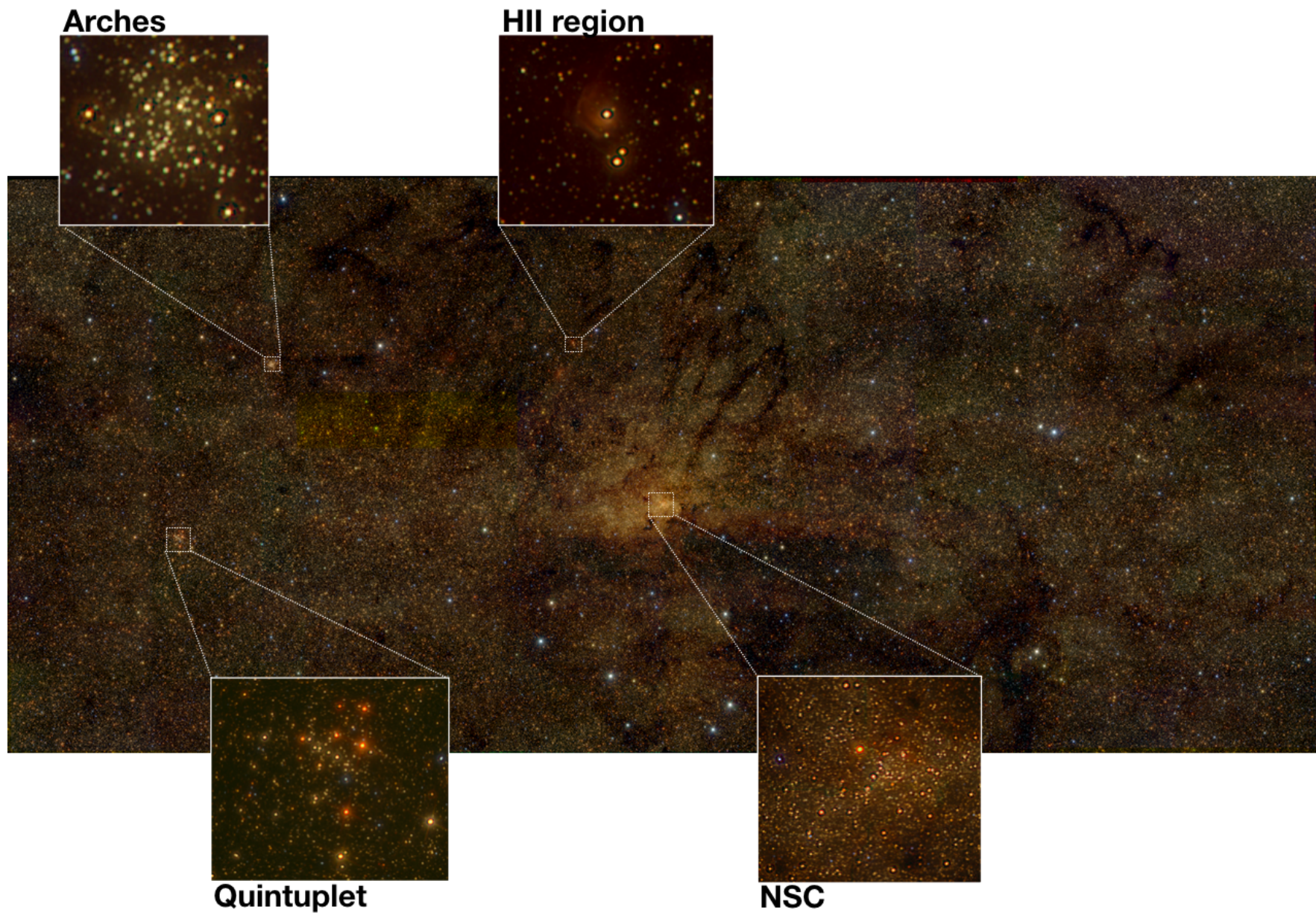


**Fig. 8.** RGB image (red =  $K_s$  band, green =  $H$  band and blue =  $J$  band) of the central catalogue corresponding to fields from 1 to 30. Field 7 is not included in  $J$  band since the observing conditions were not acceptable to include it in the survey. The insets show the NSC (e.g., Launhardt et al. 2002; Schödel et al. 2014; Boehle et al. 2016; Gravity Collaboration et al. 2018), the Arches cluster (e.g., Martins et al. 2008; Clarkson et al. 2012), the Quintuplet cluster (e.g., Figer et al. 1999; Najarro et al. 2009), and one of the HII regions that we observed.

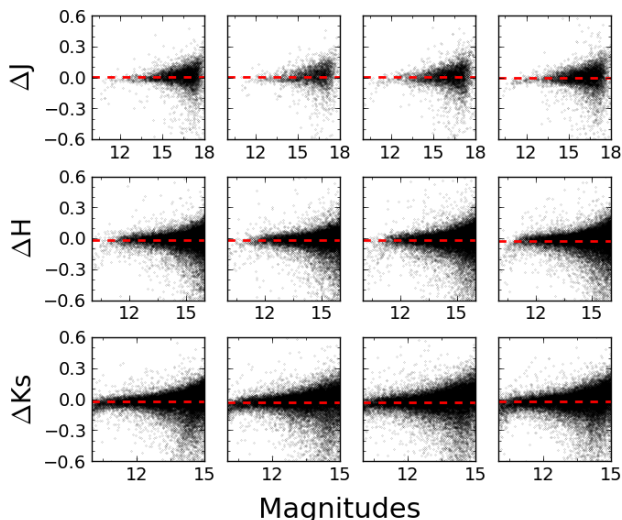


**Fig. 9.** Photometric comparison between GALACTICNUCLEUS and the SIRIUS IRSF survey across the central catalogue. We divided the central catalogue into 4 equal regions from east to west along the Galactic Plane, that are shown in each of the columns for all three bands. The red dashed line indicates the photometric offset.

Both catalogues agree very well as expected.

### 5.3. Comparison with VVV

Up to now, the most complete multi-band catalogue to study the GC was the VVV survey (Minniti et al. 2010; Saito et al. 2012). This survey covers an area of 520 deg<sup>2</sup> in the Galactic Bulge and a section of the mid-plane with high star formation activity. It uses aperture photometry to characterise  $\sim 10^9$  sources in the NIR. Since the  $JHK_s$  filters are very close to the GALACTICNUCLEUS ones, we have compared the photometry of common stars to analyse the systematics of the ZP and the data quality of our survey. We have used the VVV aperture photometry computed in a radius of 1". To calculate the ZP offset, we removed all the stars with an uncertainty  $> 0.05$  mag in both catalogues and in all three bands. Due to the extreme source crowding in the  $H$  and  $K_s$  bands, we excluded all stars with a fainter counterpart detected in GALACTICNUCLEUS within a radius of 1". We used a two sigma clipping algorithm to remove outliers and avoided saturated and too faint stars as indicated by the red dots in Fig. 11. We obtained that the small shifts agree with the systematic uncertainties estimated for the ZP. Moreover, we checked that a comparison between SIRIUS and VVV gives a similar result.

On the other hand, we compared the  $J$ ,  $H$  and  $K_s$  luminosity functions (LFs) from VVV, SIRIUS and GALACTICNUCLEUS obtained for the central catalogue (Fig. 12). GALACTICNUCLEUS reaches  $\geq 1$  mag deeper in  $J$  and  $\geq 2$  mag in  $H$  and  $K_s$ . The GALACTICNUCLEUS survey therefore improves significantly the number of stars detected at the faint end of the  $H$  and  $K_s$  LFs. The GALACTICNUCLEUS LFs are also more complete at the bright end, where the VVV survey suffers from far stronger saturation (green bumps at the bright end in Fig. 11) because of the larger pixel scale of VIRCAM and the longer exposure time used in VVV. In particular, the GALACTICNUCLEUS catalogue covers completely the red clump (RC) bump in  $K_s$ . RC stars are important standard candles and tracers of

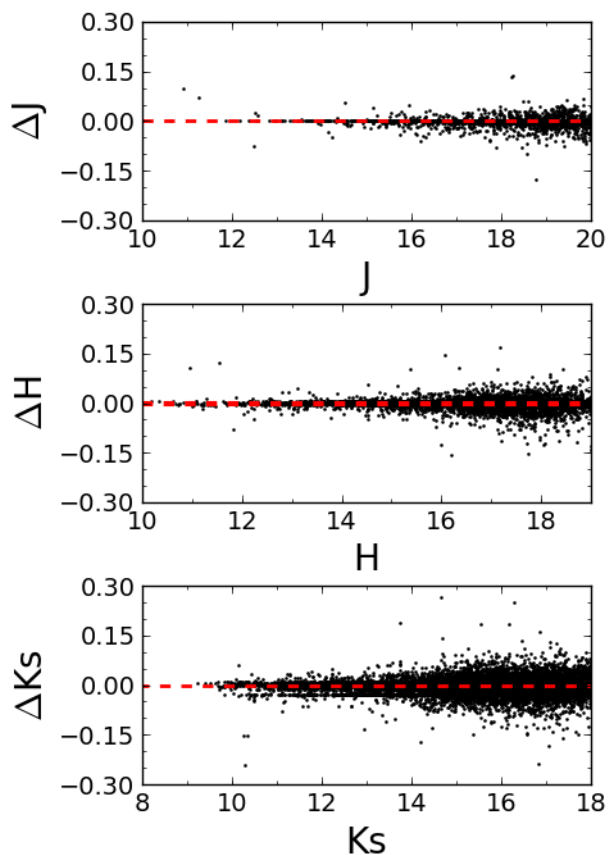


**Fig. 10.** Photometric comparison between the final version of the central catalogue of GALACTICNUCLEUS and a preliminary version obtained using the fields from 1-15 (except field 7). The red dashed line indicates the offset between the photometric ZPs.

Galactic structure. Multiple RC bumps can give information on recent star formation events or on different overlapping structures along the line-of-sight (e.g., Girardi 2016). It can be also seen that the SIRIUS survey appears as a better reference for photometric calibration in comparison to the VVV catalogue since it is far less saturated and covers a larger magnitude range in  $H$  and  $K_s$  bands.

Finally, we compared a region in the central catalogue (centred on  $17^h 45^m 47.524^s$ ,  $-28^\circ 55' 11.847''$  and covering an area of  $\sim 20' \times 17'$ ) with the recent update of the VVV survey using PSF photometry (Alonso-García et al. 2018). We obtained that the VVV photometry is quite incomplete in the bright part and does not improve the faint end of the LFs obtained using the aperture photometry. This is mainly because the new release of the catalogue only accepts a star if it is detected in at least three bands (out of  $Z, Y, J, H, K_s$ ). Moreover, this survey has not been specially designed for the GC. For the same region we also compared the photometric uncertainties given by the VVV survey with PSF photometry and GALACTICNUCLEUS. We analysed both catalogues in the same magnitude range to avoid a bias due to the different completeness limits. Therefore, we considered only stars with  $J < 19$  mag,  $H < 16$  mag and  $K_s < 14$  mag. We obtained a mean uncertainty of  $\Delta_J = 0.06$  mag,  $\Delta_H = 0.02$  mag and  $\Delta_{K_s} = 0.02$  mag for VVV and  $\Delta_J = 0.02$  mag,  $\Delta_H = 0.01$

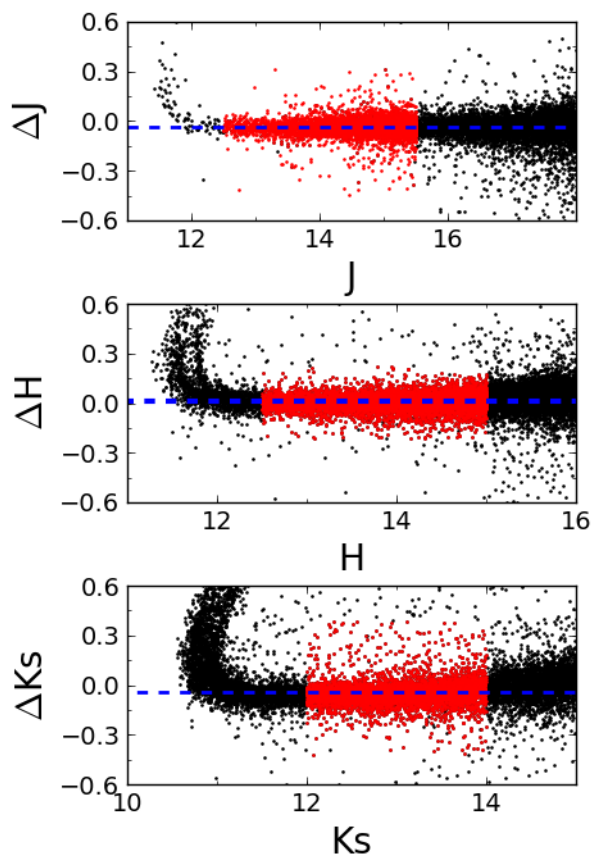


**Fig. 11.** Photometric comparison between the final version of the central catalogue of GALACTICNUCLEUS and a the VVV catalogue with aperture photometry. The red dots indicate the stars used to compute the offset. The blue dashed line corresponds to the photometric offset between both catalogues. The bright tails are due to the strong saturation in the VVV catalogue.

and  $\Delta_{K_s} = 0.01$  mag for GALACTICNUCLEUS. This supposes an improvement of factors two to three.

#### 5.4. Comparison with NICMOS HST

We compared our data with the NICMOS HST survey carried out by Dong et al. (2011) using the narrow band filters F187 and F190. We selected a common region between both catalogues of  $\sim 20' \times 10'$  centred on SgrA\*. We detected around three times more sources in the GALACTICNUCLEUS survey. We also compared the uncertainties and obtained that the relative uncertainty of the NICMOS HST survey is  $\sim 6\%$  for F187 and  $\sim 5\%$  for F190, whereas we reached a relative median uncertainty of  $\sim 2\%$  in all three bands for GALACTICNUCLEUS. Moreover, we are able to achieve the same angular resolution,  $\sim 0.2''$  using a ground based telescope. Figure 13 shows the comparison between the NSC as it is seen by NICMOS and by GALACTICNUCLEUS.

#### 5.5. Detailed analysis of pointing F1

Additional tests were carried out for the most crowded field (pointing F1) in the first paper of this series (Nogueras-Lara et al.

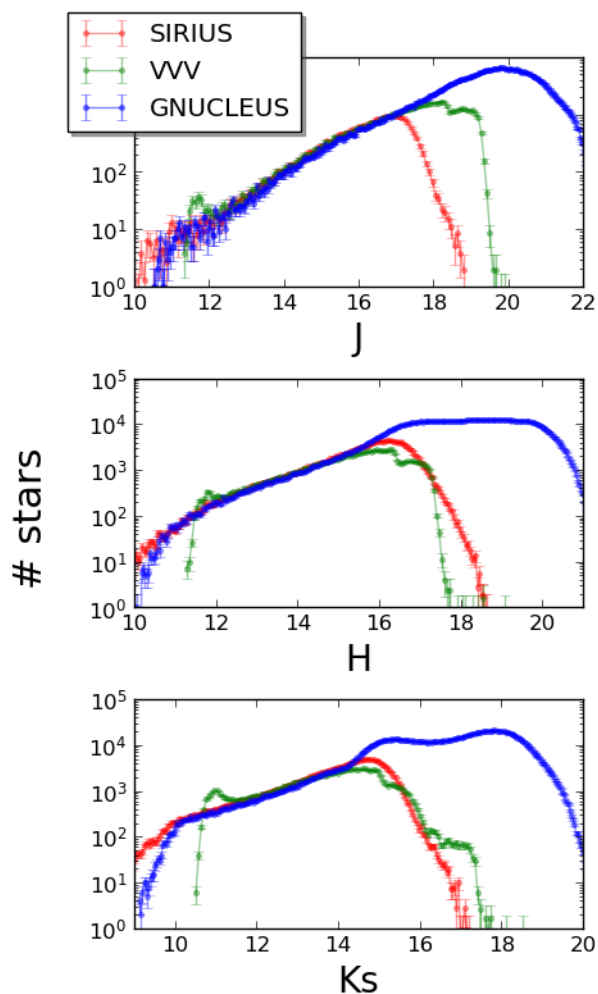


**Fig. 12.** Luminosity functions obtained with the SIRIUS survey (in red), the VVV survey (in green) and the GALACTICNUCLEUS survey (in blue). The uncertainties are Poisson errors (square root of the number of stars in each bin).

2018a). We checked the photometry and the photometric uncertainties comparing the field with previous data from 2013, we used calibration stars to check the variation of the ZP across each detector, and we estimated the uncertainties using simulations to test the influence of the extreme crowding on the photometric errors. In general all the conclusions obtained for pointing F1 can be used as upper limits for the rest of the fields under the same observing conditions.

## 6. Limitations of the survey

As it was shown previously, the GALACTICNUCLEUS catalogue supposes a great improvement in the state of art to get to know the stellar structure and population of the nuclear bulge of the Milky Way. In spite of this, there are two main limitations that need to be taken into account.

- **Photometric saturation:** in spite of the short exposure times used for the observations, the very good seeing conditions (see tables A.1, A.2 and A.3) provoke a significant saturation of the bright sources in  $K_s$  band. To study this effect, we have

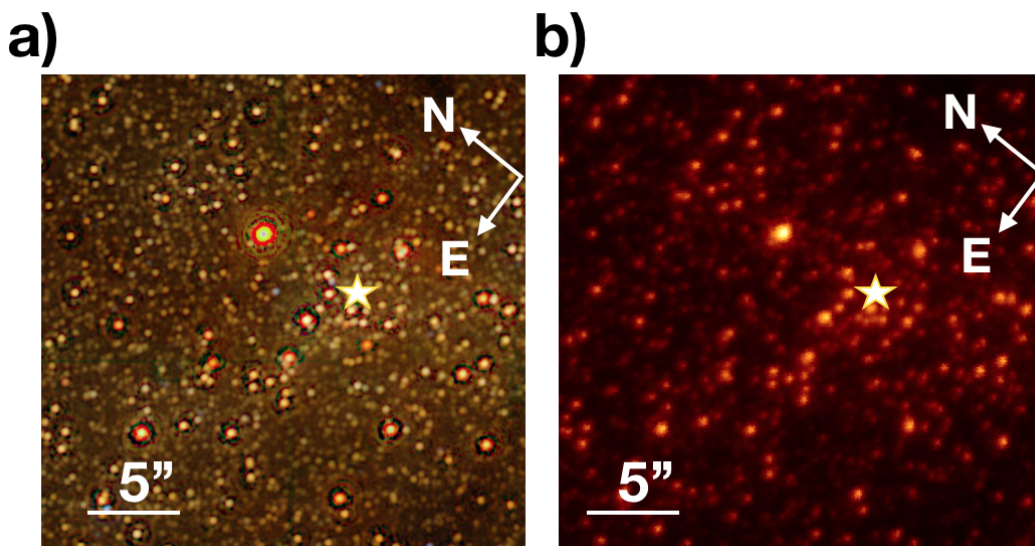


**Fig. 13.** Comparison of the NSC between (a) GALACTICNUCLEUS ( $JHK_s$  RGB image) and NICMOS HST F190 (b). The white star indicates the position of SgrA\*.

created  $K_s$  LFs using GALACTICNUCLEUS and SIRIUS data. Because of the smaller size of the telescope used for SIRIUS (1.4 m), the effect of saturation is less important in comparison to GALACTICNUCLEUS. This comparison shows that for  $K_s \sim 11.5$  mag the GALACTICNUCLEUS photometry is not reliable (see Fig. 6). Saturation is less important at  $H$  and almost negligible at  $J$ .

- **Restrictive criterion for accepting stars:** in order to estimate the uncertainties for individual stars and to avoid spurious detections, we have imposed that only stars detected in all three sub-images (see section 3) are accepted (see also Nogueras-Lara et al. 2018a). This can produce an estimated loss of  $\sim 30-40\%$  of the total number of stars present in the final holographic products. We are working on a bootstrapping algorithm to estimate the uncertainties and to obtain a deeper photometry improving the threshold for the detection of faint stars, to be published later.

## 7. Color-magnitude diagrams

The GALACTICNUCLEUS survey covers regions in the inner bulge, the NB and the transition region between them. The different stellar populations in these regions combined with the highly variable interstellar extinction result in significant differences between the corresponding color-magnitude diagrams (CMDs). Figure 14 shows the CMDs obtained for the GC Central, the Transition East and the Inner Bulge South catalogues (columns one, two and three, respectively). Typical types of stars found in the CMD are specified in the central panel: The foreground population ( $J-H \lesssim 2$  mag,  $J-K_s \lesssim 3$  mag and  $H-K_s \lesssim 1$  mag) corresponds to stars along the line-of-sight from Earth to the GC probably tracing three spiral arms (Nogueras-Lara et al. 2018a). The stellar population located at  $J-H \sim 2-3$  mag,  $J-K_s \sim 3-5$  mag,  $H-K_s \sim 1-2$  mag and  $H \sim 15$  mag and  $K_s \sim 13$  mag is composed of stars in the asymptotic giant branch (AGB) bump. The prominent feature located at  $J-H \sim 2-3$  mag,  $J-K_s \sim 3-5$  mag,  $H-K_s \sim 1-2$  mag and  $H \sim 16$  mag and

$K_s \sim 15$  mag corresponds to the RC (giant stars in their Helium core burning sequence Girardi 2016) and the red giant branch bump (RGBB, see, e.g., Cassisi & Salaris 1997; Salaris et al. 2002; Nataf et al. 2014; Nogueras-Lara et al. 2018b). Previous studies analysing regions from the Galactic bulge at higher latitudes ( $\sim 1^\circ$ ) also found a secondary RC feature and identified it as a stellar population tracing a spiral arm beyond the GC (Gonzalez et al. 2011, 2018). This feature coincides with what we here identify as the RGBB. Nevertheless, given the extreme stellar density and crowding in the low latitude regions covered by the GALACTICNUCLEUS survey, it is very unlikely to observe any star beyond the GC. Moreover our previous work (Nogueras-Lara et al. 2018b) shows that the observed feature is compatible with the RGBB. The RC and the RGBB are of great interest since their relative properties can allow us to constrain the metallicity and age of the stellar population in the sample (e.g., Nogueras-Lara et al. 2018b). Finally, stars located at  $K_s \gtrsim 17$  mag and below the RC and the RGBB belong to the ascending giant branch and post-main sequence.

## 8. Conclusions

We present the first public data release of the GALACTICNUCLEUS survey, a high angular resolution ( $0.2''$ ) a  $JHK_s$  NIR imaging survey specially designed to study the GC. The surveyed area is  $\sim 0.3$  square degrees, which corresponds to  $\sim 6000$  pc<sup>2</sup>. We describe in detail the reduction and analysis process from the raw images to the final photometric catalogue. We obtained accurate photometry for more than 3 million stars superseding previous surveys for the GC and reaching  $J \sim 1$  mag and  $H, K_s \gtrsim 2$  mag deeper than the so far best catalogues for the same region. We reached  $5\sigma$  detection limits of  $J \sim 22$  mag,  $H \sim 21$  mag and  $K_s \sim 21$  mag. The uncertainty of the photometric ZP is  $\lesssim 0.04$  mag in all bands. Relative photometric uncertainties are  $\lesssim 0.05$  mag at  $J \lesssim 21$  mag,  $H \lesssim 19$  mag and  $K_s \lesssim 18$  mag. The absolute astrometric uncertainty is  $\sim 0.05''$ . All relative astrometric positions in the final catalogue are  $< 0.05''$ . We note that the relative astrometric positions between stars on individual

chips for any given pointing are more than an order of magnitude smaller, typically only  $\sim 1$  milli-arcsecond for moderately bright stars. However, the uncertainties increase when combining the chips and pointings to the final catalogue.

We present what are probably the most complete CMDs of the GC so far, covering a large area and different regions in the nuclear stellar disc and inner bulge. The CMDs show clear differences caused by differential extinction and distinct stellar populations. We identified the foreground population, the AGBB, the post main sequence, the ascending giant branch and cover the RC and the RGBB.

Sharing our catalogue with the community, we expect to widen its usage and make it useful to solve a variety of problems and unknown questions related to the stellar population and structure of the innermost part of the Milky Way.

*Acknowledgements.* The research leading to these results has received funding from the European Research Council under the European Union's Seventh Framework Programme (FP7/2007-2013) / ERC grant agreement n° [614922]. This work is based on observations made with ESO Telescopes at the La Silla Paranal Observatory under programmes IDs 195.B-0283 and 091.B-0418. We thank the staff of ESO for their great efforts and helpfulness. Author F N-L acknowledges financial support from the State Agency for Research of the Spanish MCIU through the "Center of Excellence Severo Ochoa" award for the Instituto de Astrofísica de Andalucía (SEV-2017-0709). F N-L acknowledges financial support from a MECD pre-doctoral contract, code FPU14/01700. F N acknowledges financial support through Spanish grants ESP2015-65597-C4-1-R and ESP2017-86582-C4-1-R (MINECO/FEDER). N.N. acknowledges support by Sonderforschungsbereich SFB 881 'The Milky Way System' (subproject B8) of the German Research Foundation (DFG).

## References

- Alonso-García, J., Saito, R. K., Hempel, M., et al. 2018, *A&A*, 619, A4  
 Boehle, A., Ghez, A. M., Schödel, R., et al. 2016, *ApJ*, 830, 17  
 Cassisi, S. & Salaris, M. 1997, *MNRAS*, 285, 593  
 Clarkson, W. I., Ghez, A. M., Morris, M. R., et al. 2012, *ApJ*, 751, 132  
 Crocker, R. M. 2012, *MNRAS*, 423, 3512  
 Diolaiti, E., Bendinelli, O., Bonaccini, D., et al. 2000, *A&AS*, 147, 335  
 Dong, H., Wang, Q. D., Cotera, A., et al. 2011, *MNRAS*, 417, 114  
 Eisenhauer, F., Quirrenbach, A., Zinnecker, H., & Genzel, R. 1998, *ApJ*, 498, 278  
 Figer, D. F., McLean, I. S., & Morris, M. 1999, *ApJ*, 514, 202  
 Fritz, T. K., Gillessen, S., Dodds-Eden, K., et al. 2011, *ApJ*, 737, 73  
 Gallego-Cano, E., Schödel, R., Dong, H., et al. 2018, *A&A*, 609, A26  
 Girardi, L. 2016, *ARA&A*, 54, 95  
 Gonzalez, O. A., Minniti, D., Valenti, E., et al. 2018, *MNRAS*, 481, L130  
 Gonzalez, O. A., Rejkuba, M., Minniti, D., et al. 2011, *A&A*, 534, L14  
 Gravity Collaboration, Abuter, R., Amorim, A., et al. 2018, *A&A*, 615, L15  
 Harayama, Y., Eisenhauer, F., & Martins, F. 2008, *ApJ*, 675, 1319  
 Kissler-Patig, M., Pirard, J.-F., Casali, M., et al. 2008, *A&A*, 491, 941  
 Launhardt, R., Zylka, R., & Mezger, P. G. 2002, *A&A*, 384, 112  
 Martins, F., Hillier, D. J., Paumard, T., et al. 2008, *A&A*, 478, 219  
 Mauerhan, J. C., Munro, M. P., Morris, M. R., Stolovy, S. R., & Cotera, A. 2010, *ApJ*, 710, 706  
 Minniti, D., Lucas, P. W., Emerson, J. P., et al. 2010, *New A*, 15, 433  
 Morris, M. & Serabyn, E. 1996, *ARA&A*, 34, 645  
 Nagayama, T., Nagashima, C., Nakajima, Y., et al. 2003, in *Proc. SPIE*, Vol. 4841, Instrument Design and Performance for Optical/Infrared Ground-based Telescopes, ed. M. Iye & A. F. M. Moorwood, 459–464  
 Najarro, F., Figer, D. F., Hillier, D. J., Geballe, T. R., & Kudritzki, R. P. 2009, *ApJ*, 691, 1816  
 Nataf, D. M., Cassisi, S., & Athanassoula, E. 2014, *MNRAS*, 442, 2075  
 Nishiyama, S., Nagata, T., Kusakabe, N., et al. 2006a, *ApJ*, 638, 839  
 Nishiyama, S., Nagata, T., Sato, S., et al. 2006b, *ApJ*, 647, 1093  
 Nishiyama, S., Nagata, T., Tamura, M., et al. 2008, *ApJ*, 680, 1174  
 Nogueras-Lara, F., Gallego-Calvente, A. T., Dong, H., et al. 2018a, *A&A*, 610, A83  
 Nogueras-Lara, F., Schödel, R., Dong, H., et al. 2018b, *A&A*, 620, A83  
 Petr, M. G., Coude Du Foresto, V., Beckwith, S. V. W., Richichi, A., & McCaughrean, M. J. 1998, *ApJ*, 500, 825  
 Pfuhl, O., Fritz, T. K., Zilka, M., et al. 2011, *ApJ*, 741, 108  
 Portegies Zwart, S. F., Makino, J., McMillan, S. L. W., & Hut, P. 2002, *ApJ*, 565, 265

- Primot, J., Rousset, G., & Fontanella, J. C. 1990, *Journal of the Optical Society of America A*, 7, 1598  
 Reid, M. J. & Brunthaler, A. 2004, *ApJ*, 616, 872  
 Saito, R. K., Minniti, D., Dias, B., et al. 2012, *A&A*, 544, A147  
 Salaris, M., Cassisi, S., & Weiss, A. 2002, *PASP*, 114, 375  
 Schödel, R., Eckart, A., Alexander, T., et al. 2007, *A&A*, 469, 125  
 Schödel, R., Feldmeier, A., Kunneriath, D., et al. 2014, *A&A*, 566, A47  
 Schödel, R., Gallego-Cano, E., Dong, H., et al. 2018, *A&A*, 609, A27  
 Schödel, R., Najarro, F., Muzic, K., & Eckart, A. 2010, *A&A*, 511, A18+  
 Schödel, R., Yelda, S., Ghez, A., et al. 2013, *MNRAS*, 429, 1367  
 Scoville, N. Z., Stolovy, S. R., Rieke, M., Christopher, M., & Yusef-Zadeh, F. 2003, *ApJ*, 594, 294  
 Yusef-Zadeh, F., Hewitt, J. W., Arendt, R. G., et al. 2009, *ApJ*, 702, 178

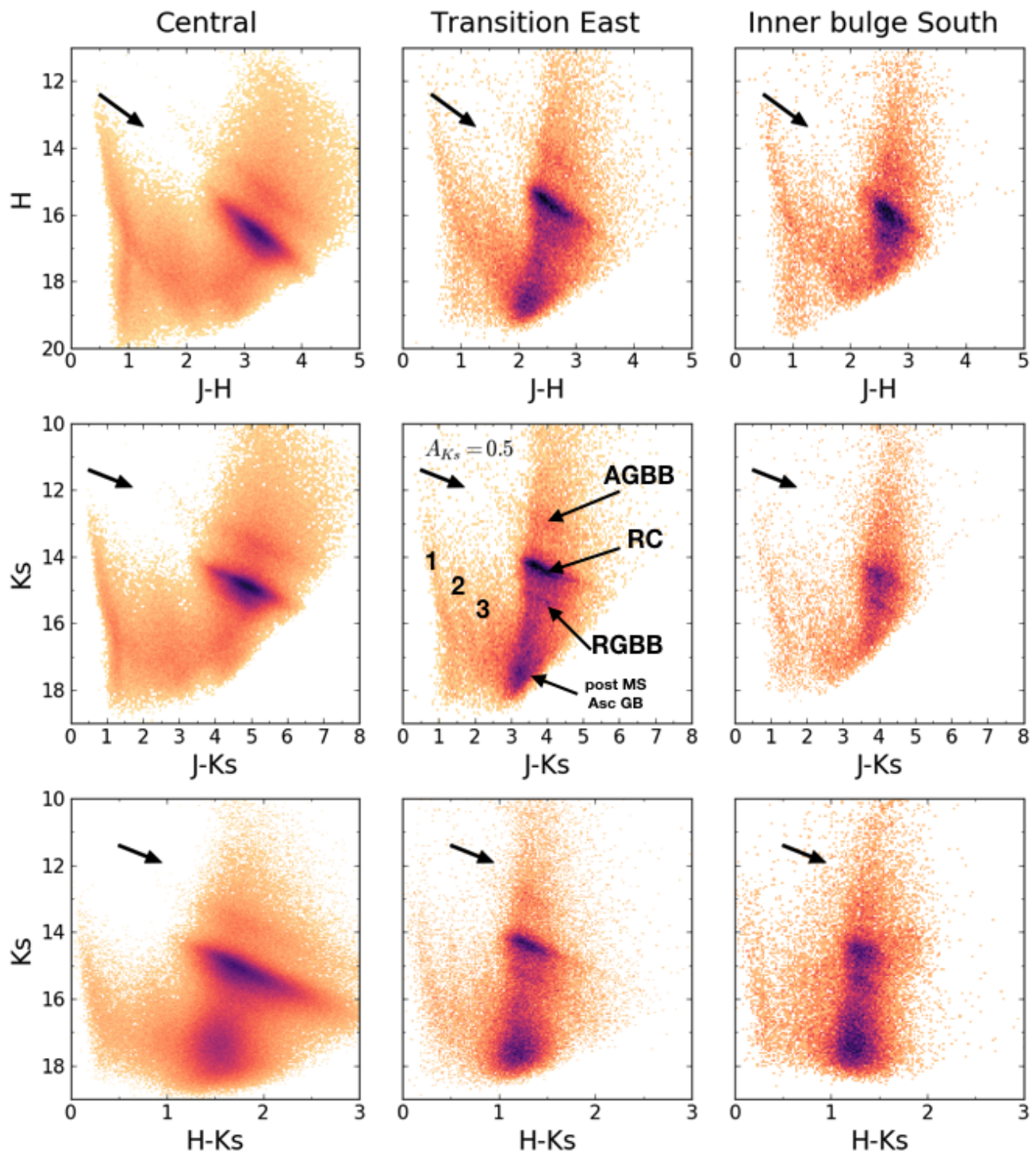


**Fig. 14.** Colour-magnitude diagrams for different regions of the GALACTICNUCLEUS survey. The colour code corresponds to stellar densities, using a power stretch scale. First, second and third columns correspond to the central, the transition East and the inner bulge South catalogues. The black arrow indicates the reddening vector and an extinction of 0.5 mag in the  $K_s$  band. The labels in the central panel correspond to the different stellar populations present in the CMDs: AGBB (asymptotic giant branch bump), RC (red clump), RGBB (red giant branch bump), post MS (post main sequence stars), Asc G B (ascending giant branch) and the numbers from 1 to 3 indicate the foreground population corresponding to three spiral arms.

## Appendix A: Tables

Tables A.1, A.2 and A.3 summarise the observing conditions of the data used to produce the GALACTICNUCLEUS survey.

**Table A.1.** Observing details for the fields used for the central catalogue.

HAWK-I filter	Field	Date (d/m/year)	Seeing <sup>a</sup> (arcsec)	N <sup>b</sup>	Field	Date (d/m/year)	Seeing <sup>a</sup> (arcsec)	N <sup>b</sup>	Field	Date (d/m/year)	Seeing <sup>a</sup> (arcsec)	N <sup>b</sup>
<i>J</i>		08/06/2015	0.37	49		06/06/2015	0.58	49		08/06/2015	0.40	49
<i>H</i>	F1	06/06/2015	0.52	49	F2	06/06/2015	0.70	48	F3	06/06/2015	0.73	49
<i>K<sub>s</sub></i>		06/06/2015	0.57	49		07/06/2015	0.60	49		06/06/2015	0.60	49
<i>J</i>		06/06/2015	0.76	49		06/06/2015	0.58	49		07/06/2015	0.57	49
<i>H</i>	F4	06/06/2015	0.74	49	F5	06/06/2015	0.60	49	F6	07/06/2015	0.63	49
<i>K<sub>s</sub></i>		06/06/2015	0.86	49		07/06/2015	0.55	49		07/06/2015	0.53	49
<i>J</i>		-	-	-		07/06/2015	0.57	49		08/06/2015	0.40	49
<i>H</i>	F7	07/06/2015	0.47	50	F8	07/06/2015	0.56	49	F9	08/06/2015	0.40	49
<i>K<sub>s</sub></i>		10/06/2018	0.62	49		08/06/2015	0.60	48		08/06/2015	0.54	49
<i>J</i>		08/06/2015	0.35	49		08/06/2015	0.36	49		08/06/2015	0.36	49
<i>H</i>	F10	08/06/2015	0.46	49	F11	09/06/2015	0.47	49	F12	09/06/2015	0.43	49
<i>K<sub>s</sub></i>		08/06/2015	0.45	49		09/06/2015	0.62	49		09/06/2015	0.62	49
<i>J</i>		09/06/2015	0.46	49		09/06/2015	0.40	49		10/06/2015	0.53	49
<i>H</i>	F13	09/06/2015	0.45	48	F14	09/06/2015	0.53	48	F15	10/06/2015	0.62	49
<i>K<sub>s</sub></i>		09/06/2015	0.48	49		09/06/2015	0.66	49		10/06/2015	0.64	49
<i>J</i>		10/06/2015	0.48	49		10/06/2015	0.52	49		27/06/2015	0.47	48
<i>H</i>	F16	10/06/2015	0.46	47	F17	10/06/2015	0.60	48	F18	27/06/2015	0.32	49
<i>K<sub>s</sub></i>		10/06/2015	0.55	49		10/06/2015	0.57	48		04/07/2015	0.66	49
<i>J</i>		27/06/2015	0.34	49		27/06/2015	0.33	49		27/06/2015	0.39	48
<i>H</i>	F19	27/06/2015	0.38	49	F20	21/07/2015	0.47	49	F21	21/07/2015	0.62	49
<i>K<sub>s</sub></i>		02/07/2015	0.45	49		05/07/2015	0.76	48		12/07/2015	0.53	49
<i>J</i>		12/07/2015	0.42	49		12/07/2015	0.41	49		19/07/2015	0.38	49
<i>H</i>	F22	21/07/2015	0.73	47	F23	24/07/2015	0.41	48	F24	25/07/2015	0.60	49
<i>K<sub>s</sub></i>		13/07/2015	0.56	49		13/07/2015	0.51	49		13/07/2015	0.68	48
<i>J</i>		19/07/2015	0.41	49		21/07/2015	0.64	49		21/07/2015	0.59	41
<i>H</i>	F25	24/07/2015	0.62	46	F26	25/07/2015	0.88	48	F27	03/10/2015	0.51	49
<i>K<sub>s</sub></i>		25/07/2015	0.67	49		25/07/2015	0.72	51		18/09/2015	0.49	49
<i>J</i>		20/07/2015	0.46	49		23/07/2015	0.45	49		24/07/2015	0.43	49
<i>H</i>	F28	04/10/2015	0.50	49	F29	27/03/2016	0.59	50	F30	20/05/2016	0.56	48
<i>K<sub>s</sub></i>		27/03/2016	0.60	30		12/05/2016	0.67	47		07/10/2015	0.74	48

**Notes.** (a) In-band seeing estimated from the PSF FWHM measured in long exposure images. (b) Number of pointings. The data corresponding to F7 (*J* band) were obtained under bad conditions and have not been included in the final data release of the survey.

**Table A.2.** Observing details for the fields used for the inner bulge and the transition zone.

Filter	Field	Date (d/m/year)	Seeing <sup>a</sup> (arcsec)	N <sup>b</sup>
<i>J</i>		24/07/2015	0.43	49
<i>H</i>	B1	20/05/2016	0.56	49
<i>K<sub>s</sub></i>		28/06/2015	0.54	49
<i>J</i>		24/07/2015	0.43	49
<i>H</i>	B2	26/05/2016	0.33	49
<i>K<sub>s</sub></i>		14/05/2016	0.58	49
<i>J</i>		24/07/2015	0.39	51
<i>H</i>	T3	21/05/2016	0.51	50
<i>K<sub>s</sub></i>		14/05/2016	0.47	50
<i>J</i>		27/06/2016	0.46	49
<i>H</i>	T4	12/06/2016	0.79	49
<i>K<sub>s</sub></i>		12/06/2016	0.56	50
<i>J</i>		27/06/2016	0.48	49
<i>H</i>	B5	12/06/2016	0.83	49
<i>K<sub>s</sub></i>		12/06/2016	0.95	30
<i>J</i>		27/06/2016	0.51	49
<i>H</i>	B6	-	-	-
<i>K<sub>s</sub></i>		05/04/2017	0.46	44
<i>J</i>		27/06/2016	0.55	49
<i>H</i>	T7	24/04/2017	0.42	38
<i>K<sub>s</sub></i>		26/06/2016	0.73	49
<i>J</i>		27/06/2016	0.56	49
<i>H</i>	T8	27/06/2016	0.54	59
<i>K<sub>s</sub></i>		02/05/2017	0.64	43

**Notes.** (a) In-band seeing estimated from the PSF FWHM measured in long exposure images. (b) Number of pointings. The data corresponding to B6 (H band) were obtained under bad conditions and have not been included in the final data release of the survey.

**Table A.3.** Observing details for the fields used for the NSD.

Filter	Field	Date	Seeing <sup>a</sup>	N <sup>b</sup>	Field	Date	Seeing <sup>a</sup>	N <sup>b</sup>	Field	Date	Seeing <sup>a</sup>	N <sup>b</sup>
		(d/m/year)	(arcsec)			(d/m/year)	(arcsec)			(d/m/year)	(arcsec)	
<i>J</i>		27/06/2016	0.49	49		27/06/2016	0.81	49		28/06/2016	0.87	48
<i>H</i>	D9	27/06/2016	1.13	49	D10	28/06/2016	0.91	49	D11	28/06/2016	0.89	49
<i>K<sub>s</sub></i>		03/05/2017	0.77	50		27/06/2016	0.81	48		28/06/2016	0.90	49
<i>J</i>		20/07/2017	0.51	44		23/09/2017	0.54	44		30/09/2017	0.49	44
<i>H</i>	D12	03/06/2017	0.33	44	D13	24/06/2017	0.70	44	D14	23/07/2017	0.66	44
<i>K<sub>s</sub></i>		03/06/2017	0.35	39		24/06/2017	0.61	48		11/08/2017	0.65	44
<i>J</i>		01/10/2017	0.85	44		27/03/2018	0.41	44		21/05/2018	0.38	44
<i>H</i>	D15	21/09/2017	0.75	44	D17	22/03/2018	0.34	43	D18	28/03/2018	0.82	47
<i>K<sub>s</sub></i>		11/08/2017	0.85	44		27/03/2018	0.37	43		28/03/2018	0.79	44
<i>J</i>		25/05/2018	0.49	44		10/06/2018	0.88	44				
<i>H</i>	D19	21/05/2018	0.41	44	D21	25/05/2018	0.59	44				
<i>K<sub>s</sub></i>		16/04/2018	0.54	44		06/06/2018	0.51	44				

**Notes.** (a) In-band seeing estimated from the PSF FWHM measured in long exposure images. (b) Number of pointings.